

RESEARCH ARTICLE | SEPTEMBER 03 2025

Effects of particle shape on the jamming and rheological behavior of granular spreading flow

Ziming He  ; Wenguang Nan   ; Rui Ma; Lanzhou Ge; Yi He



Physics of Fluids 37, 093308 (2025)
<https://doi.org/10.1063/5.0283620>



Articles You May Be Interested In

Particle fluctuations and their effects on the rheological behavior of sheared granular flows

Physics of Fluids (June 2023)

Rheological behaviour on Polypropylene-Nanoclay-Gigantochloa Scortechnii fibres

AIP Conf. Proc. (May 2023)

DEM Simulation of Granular Flows on a Heap

AIP Conf. Proc. (June 2009)

Effects of particle shape on the jamming and rheological behavior of granular spreading flow

Cite as: Phys. Fluids **37**, 093308 (2025); doi: [10.1063/5.0283620](https://doi.org/10.1063/5.0283620)

Submitted: 2 June 2025 · Accepted: 11 August 2025 ·

Published Online: 3 September 2025



View Online



Export Citation



CrossMark

Ziming He,¹ Wenguang Nan,^{1,2,a)} Rui Ma,³ Lanzhou Ge,¹ and Yi He⁴

AFFILIATIONS

¹School of Mechanical and Power Engineering, Nanjing Tech University, Nanjing 211816, China

²Faculty of Engineering and Physical Sciences, University of Leeds, Leeds LS2 9JT, United Kingdom

³KOCEL Intelligent Machinery Limited, Yinchuan 750021, China

⁴TenFong Technology Co., Ltd, Shenzhen 518055, China

^{a)}Author to whom correspondence should be addressed: nanwg@njtech.edu.cn

ABSTRACT

Granular spreading flow is explored through experiments and simulations using the discrete element method (DEM), in which a particle heap on a base is spread through a narrow gap by a moving blade, with the formation of a thin layer on the base. A large rolling friction is used for spherical particles in the DEM simulation, for which a similar flowability as angular particles could be obtained. The results show that different styles of empty patches could be formed on the base, which are related to the spatial structure of intermittent jamming. High localized stress generated during the survival period of jamming could even induce the breakage of particles in brittle material. Interlocking between the particles and the blade or the base is important for mechanical jamming, and the critical gap size for the particle flow without any jamming events increases when the particles with a strong rolling resistance are involved. The shear band mainly exists in the bottleneck region, and its velocity distribution could be well described by the Gauss error function as used in the split-bottom Couette cell. The width of the shear band of angular particles is much restricted by the stationary base when the gap size is small. A separation point exists in the bottleneck region in terms of particle vertical velocity, and its position is related to the blade tip. Because of the combined effects of blade shearing and bottleneck effect, the bulk friction coefficient in this work is larger than that of a traditional shearing flow system.

Published under an exclusive license by AIP Publishing. <https://doi.org/10.1063/5.0283620>

I. INTRODUCTION

Reliable control of granular flow through constrictions is of great interest in particle processing industries. The narrow clearance of constrictions would cause problems with granular flow, such as jamming and clogging.^{1,2} The jamming of granular flow through constrictions has been extensively studied in several granular systems, such as hopper flow driven by gravity^{2–4} as affected by the number of outlets⁵ and external vibration,⁶ belt flow driven by friction,^{7,8} pipe flow driven by fluid,⁹ in which the outlet would be finally blocked with the permanent halting of particle flow. The underlying physics of jamming in these granular systems, such as the critical size of constrictions and the mathematical model of jamming probability, has been explored through both experiments and simulations, as reviewed by Behringer *et al.*¹⁰ and Pan *et al.*¹¹

Recently, another kind of granular system, i.e., a particle heap is spread onto a rough work surface to form a thin layer by using a moving blade over it, has attracted significant attention from researchers and industry due to its wide application in powder-based additive

manufacturing.¹² In this system, under the combined effects of the narrow clearance between the blade tip and work surface and the shearing effects of the moving blade, jamming and clogging of particles would intermittently and transiently occur, as reported by Nan *et al.*¹³ using the discrete element method (DEM) and their following experimental work.¹⁴ They proposed a regime map of jamming for a granular spreading system, depending on the gap size of constriction as normalized by particle diameter, the particle interlocking caused by irregular particle shape, and the particle cohesion. Meanwhile, particle jamming plays an important role in the wear of the blade¹⁵ and the formation of defects within the spread layer, such as empty patches¹⁶ and particle segregation.^{17,18} However, there is still a lack of a good understanding of the physics of jamming in granular spreading systems, including the jamming-induced empty patches and the jamming structure, as well as the related rheology, especially for the particles with irregular shapes. Xu *et al.*¹⁹ highlighted the importance of particle rolling on the stability of the jamming structure, but they used spherical particles with very large rolling friction instead of the realistic angular-shaped particles in their DEM simulation.

In this work, the jamming and rheological behavior of angular particles in the granular spreading system is explored through experiments and DEM simulations, in which a particle heap is thinly spread onto a base by a moving plate over it, in which the gap between the blade tip and base surface is comparable to the particle size. The results are compared with those of spherical particles under the same spreading conditions. The jamming-induced empty patches and particle breakage are first identified by experiments, followed by the reproduction using DEM simulations. The difference in the jamming behavior between the angular particles and the spherical particles is explored, followed by their sensitivity to the roughness of the base. The velocity profiles and stresses of particle flow in the shearing band are also explored, followed by the development of their mathematical models. The results will have a notable impact on the further understanding of the nature of jamming and rheology in granular systems and its application in industry, such as the powder spreading processes of additive manufacturing.

II. METHODS

A. Experiment methods

The schematics of the experimental system are shown in Fig. 1, which mainly consists of a moving blade and a base with a force sensor underneath it. The clearance between the blade and the base, δ , is controlled by a micrometre caliper and calibrated by the feeler gauges. The particles are first fed into the front of the blade by a micro-vibration feeder, and then the particle heap begins to be spread onto the base by the blade at a constant speed as controlled by a servo motor. Because of the limits of the experiment system, such as the sampling frequency of the force sensor, a low spreading speed is used, i.e., $U = 0.01 \text{ m/s}$.

More details of the test rig could be referred to Nan *et al.*¹⁴ It should be noted that the particles are used only once and discarded after each experimental test, as the particle surface has the potential to be damaged, which will be further discussed in Sec. III. The particles are dried before each experimental test to avoid the effects of possible moisture during storage, and the experiment is carried out under normal atmospheric conditions. The images of the spread layer after the experiment are obtained by a CCD camera with a high resolution, and then they are merged and analyzed by using ImageJ software.²⁰

To depict the effects of particle shape on the particle jamming and spreading behavior, two kinds of fine powder used in the practical AM techniques are adopted here: 316L stainless steel powder with particle shape close to the sphere, and sand powder with particles in an angular shape, as shown in the SEM images in Fig. 1. For the first, the powder size is $D = 103 \mu\text{m}$ and it is labeled as powder A, and for the latter, the powder size is $D = 190 \mu\text{m}$ and it is labeled as powder B, in which D is the characteristic size of particles with the size distribution shown in Fig. 1. As the particle jamming in the bottleneck region of the granular spreading system is very sensitive to the presence of large particles, the characteristic particle size, i.e., D , is quantified by the number based D_{90} of the particle size distribution, at which the cumulative distribution percentage in terms of particle number reaches 90%. For powder A, the gap size is 150 and 200 μm , resulting in $\delta/D = 1.46$ and 1.94, respectively. For powder B, the gap size is 300 and 400 μm , resulting in $\delta/D = 1.58$ and 2.11, respectively. For the base, the length (i.e., the spreading direction) is 25 mm, and the width (i.e., perpendicular to the spreading direction) is 3 mm for powder A and 5 mm for powder B, respectively. The summary of the spreading conditions in the experiment is shown in Table I. It should be noted that the

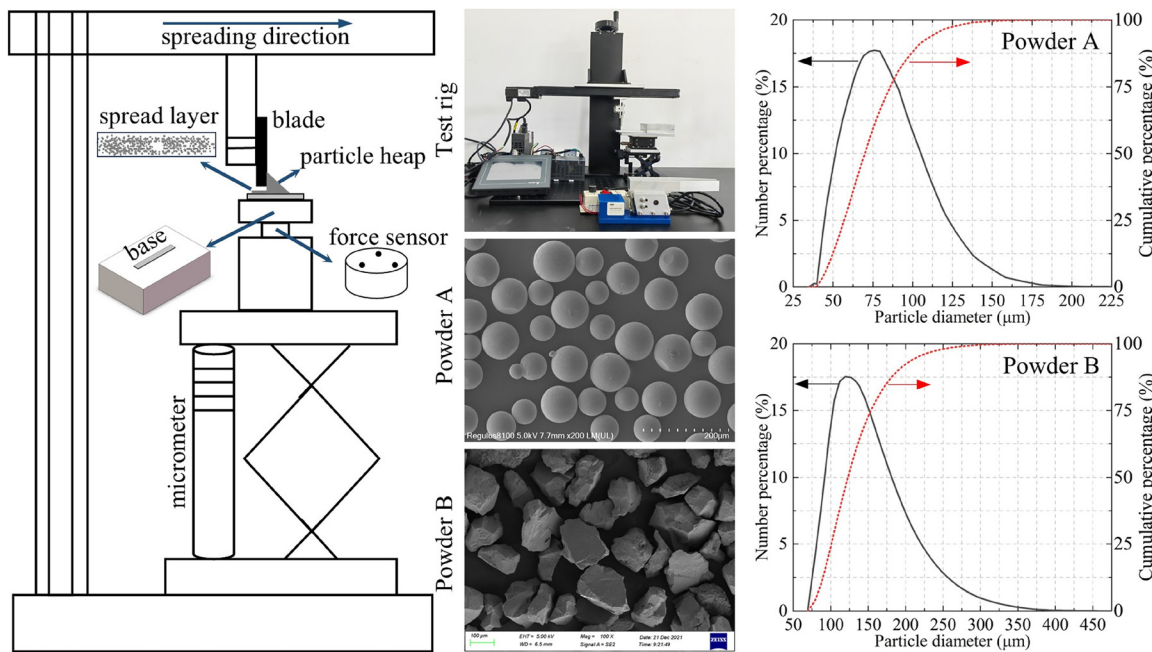


FIG. 1. Schematics of the spreading system and the SEM images and particle size distribution (PSD) of powder A (spherical particle shape) and powder B (angular particle shape) used in the experiment, in which the spread layer is referred to the particles spread onto the base through a narrow gap by using a moving blade, and the force exerted on the base during the spreading process is monitored.

spreading dynamics is significantly affected by the relative ratio of the gap size to the particle size, as demonstrated by Nan *et al.*¹³ thus, the non-dimensional parameter, δ/D , is used in this work.

B. Simulation conditions

The spreading process of powder B in the experiment is also modeled by the DEM.^{21,22} The front and rear boundaries (i.e., in the y direction) of the simulation domain are treated as periodic boundaries with a corresponding width of 3 mm. Based on the SEM image of powder B, as shown in Fig. 1, the particles are simplified as cubes in the simulation, as shown in Fig. 2, for which the angular feature of the practical particles could be guaranteed at a low computational cost. The physical and mechanical properties of particles, as needed for DEM simulation, are given in Table II. The size distribution of the particles used in the simulation is the same as the ones characterized by the experiment, as shown in the snapshot in Fig. 1. The friction angle of single particle is measured by the sliding method,^{13,23} in which a plate with the surface as glued by a very thin layer of particles is slid against a target surface. The averaged friction of particle against particle and blade/base is 0.65 and 0.44, respectively. The restitution coefficient is characterized by using the traditional gravity-induced impact test, in which the impact velocity and rebound velocity of the particle are measured by using a high-speed camera. The averaged restitution coefficient of particle against particle is assumed to be the same as that of particle against blade/base as experimentally characterized, i.e., 0.7. The initial particle heap is prepared by using the poured packing method, and then the blade is lifted vertically to generate the specified gap size δ between the blade tip and the base surface. Afterwards, the blade accelerates quickly to the specified speed, then moves forward at this constant speed, followed by a particle heap being spread onto the base. To speed up the simulation, a larger spreading speed than the experiment is adopted in the simulation, i.e., $U=0.08$ m/s, which is below the critical spreading speed [i.e., $5(gD)^{0.5}=0.22$ m/s] as predicted by Nan and Ghadiri.²⁴ Four kinds of gap size are used in the simulation, i.e., 300, 400, 500, and 600 μm , resulting in the δ/D of 1.58, 2.11, 2.63, and 3.16, respectively. A summary of the spreading conditions used in DEM simulations is shown in Table III.

For the angular particles (i.e., cubes used in this work), the contact interaction force of particle against particle/wall is described by the Hertz–Mindlin Nassauer–Kuna model, in which the magnitude of the normal contact force F_n is given as²⁵

$$F_n = E^* k \sqrt{Vd} (1 + cv''), \quad (1)$$

where E^* is the equivalent Young's modulus; k is a correction factor, and a value of 0.62 is adopted here as suggested by Nassauer and Kuna for polyhedral particles;²⁵ V is the overlap volume; d is the indentation depth, calculated as the difference between the maximum and the minimum of the projection of the coordinates of the corners of the overlapping region on the normal contact direction; v'' is the magnitude of

the relative velocity between both particles in contact in the direction of normal force; c is the damping constant. The magnitude of the tangential force F_t is given as²⁵

$$F_t = \left((2\mu_s^* - \mu_k) \frac{x^2}{x^4 + 1} + \mu_k - \frac{\mu_k}{x^2 + 1} \right) F_n, \quad (2)$$

$$\mu_s^* = \mu_s \left(1 - 0.09 \left(\frac{\mu_k}{\mu_s} \right)^4 \right), \quad (3)$$

$$x = \frac{v_t}{v_s}, \quad (4)$$

where μ_s and μ_k are the coefficients for static friction and kinetic friction, respectively; v_t is the magnitude of the tangential velocity, and v_s is the velocity for transition from static to kinetic friction.

For comparison, the spherical particles are also used in the simulation, in which the same physical and mechanical properties as listed in Table II are used. In this case, the contact interaction force of particle against particle/wall is described by the Hertz–Mindlin model.²² To obtain the same repose angle of the initial particle heap as that of angular particles in Fig. 2, a large rolling friction coefficient of 0.8 is used for spherical particles. To better model the spreading behavior of granular material consisting of predominantly angular particles using spherical particles, the rolling friction model developed by Ai *et al.*²⁶ is used instead of the standard rolling friction model. More details on the application of this method in the simplification of the modeling of non-spherical particles could be referred to Xu *et al.*¹⁹ It should be noted that the surface attrition and even breakage of particles that may occur in the experiment are not considered in the DEM simulations in this work, due to their complexities, and their influence on jamming and rheology of the granular spreading system would be explored in the future.

III. EXPERIMENT RESULTS

The images of the spread layer of powder A and powder B are shown in Figs. 3 and 4, respectively, in which the results of ten independent experimental tests are reported for each spreading condition. It could be found that there are a few empty patches with different sizes and geometrical shapes along the spreading direction, in which the empty patches refer to the local regions of the base surface that are not covered by particles. The empty patches directly describe the occurrence of jamming events. The size of the empty patches could range from a few particle diameters to a few millimeters, depending on the particle properties and spreading conditions. It is interesting that for powder A, as shown in Fig. 3, at the gap size of $1.46D$, the spread layer has a large tendency to form empty patches with a slender shape, in which the axial direction of these empty patches is consistent with the spreading direction. The elongated empty patches are more obvious when the gap size increases to $1.94D$, although the total area of empty patches shows a decrease, the underlying reasons for which are

TABLE I. Spreading conditions in the experiment.

Label	Material	Particle size, D (μm)	Gap size, δ (μm)	δ/D	Blade speed, U (m/s)
Powder A	316L stainless steel	103	150, 200	1.46, 1.94	0.01
Powder B	Sand	190	300, 400	1.58, 2.11	0.01

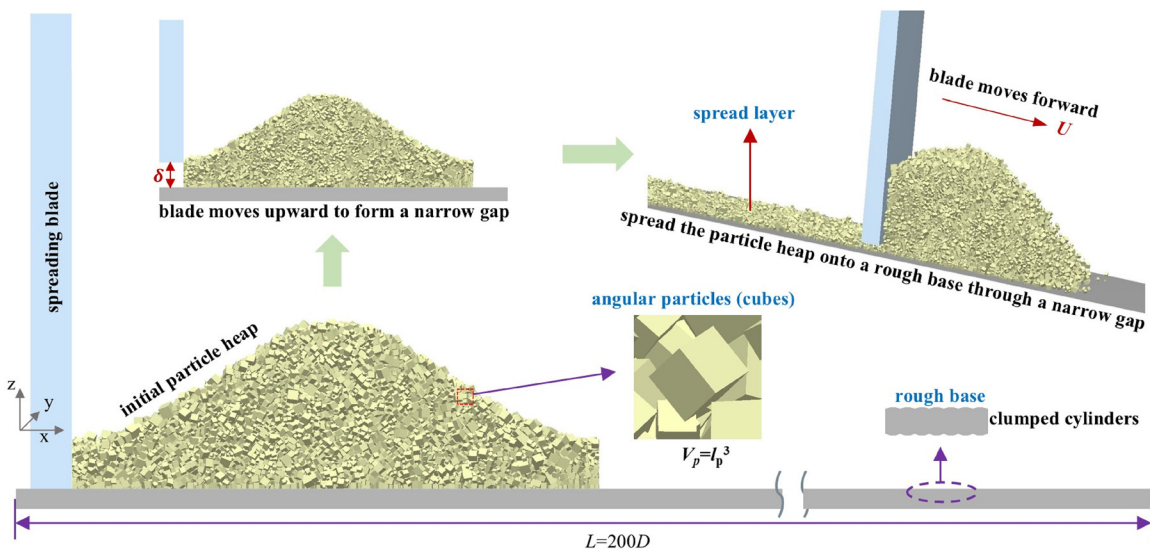


FIG. 2. Schematics of the spreading system and particles used in simulation, in which angular particles (i.e., cubes) are used for illustration.

TABLE II. Physical and mechanical properties of particles used in simulation.

Parameter	Value
Density, ρ_p (kg/m ³)	2650
Young's modulus, E (MPa)	50
Poisson's ratio	0.3
Friction coefficient, μ	0.65 ^a
Restitution coefficient, e	0.7

^a0.44 is used for particle-blade interaction.

TABLE III. Spreading conditions used in DEM simulations.

Particle shape	Particle size, D (μm)	Gap size, δ (μm)	δ/D	Blade speed, U (m/s)
Angular particle, spherical particle	190	300, 400, 500, 600	1.58, 2.11, 2.63, 3.16	0.08

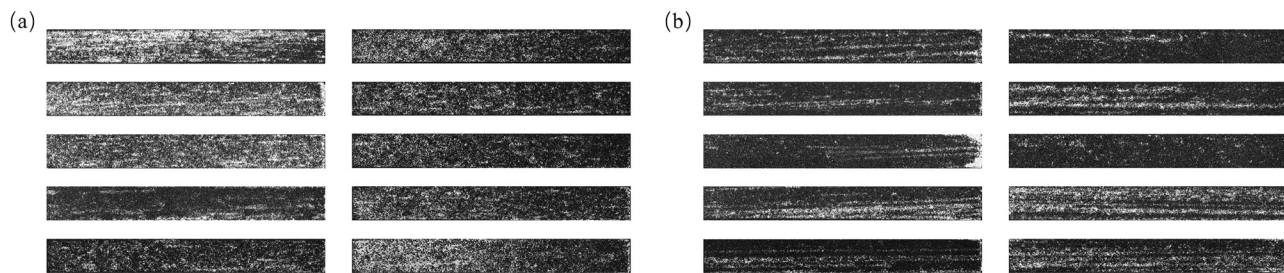


FIG. 3. Images of the spread layer of powder A (i.e., 316L stainless steel powder with almost spherical particle shape) at the gap size of (a) 1.46 D and (b) 1.94 D , in which a total of ten experiment tests are conducted for each gap size, and each image represents one experiment test.

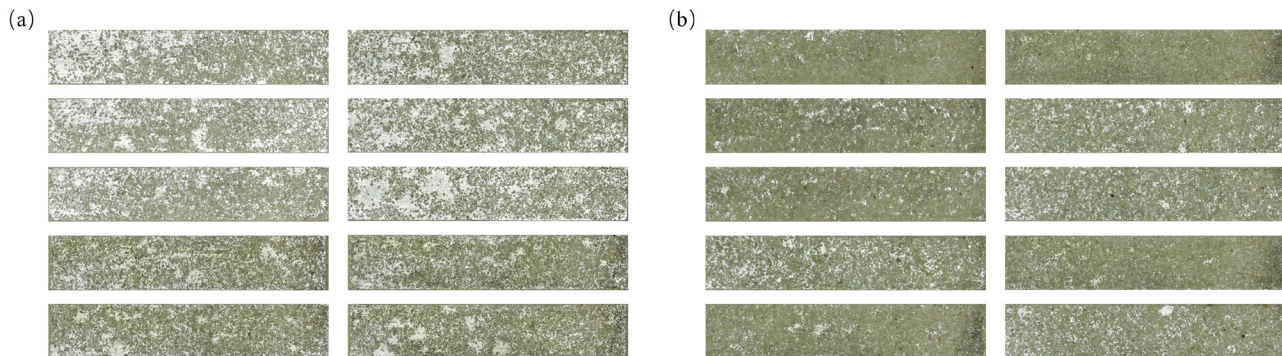


FIG. 4. Images of the spread layer of powder B (i.e., sand powder with an angular particle shape) at the gap size of (a) $1.58D$ and (b) $2.11D$, in which a total of ten experiment tests are conducted for each gap size and each image represents one experiment test.

also demonstrates the intermittent occurrence of intense mechanical jamming. It should be noted that this kind of intense mechanical jamming could cause damage to the particles, which was previously reported for the granular system in an impeller-based rheometer.²⁷ Here, to further investigate the particle damage induced by mechanical jamming that occurred in the spreading process, the particles within the size range of $212\text{--}250\,\mu\text{m}$, i.e., the size above the number-based D_{90} of powder B, are carefully sieved out from powder B, and then they are subjected to additional spreading experiments at the gap size of $300\,\mu\text{m}$. The snapshots of the particles on the base after spreading are shown in Fig. 5. It can be observed that there are a few fragmented particles, the size of which is much smaller than the surrounding particles, and one example is marked by the red square. It suggests that high localized stress formed during the survival period of the intense mechanical jamming could even induce the breakage of particles, which is prone to the angular particle in brittle material as used in this experiment. The angular particles have a strong tendency to interlock with the blade and base, and the rolling motion of particles is reduced, making the energy imposed by the blade more easily accumulated on the particle and finally exceeding the value required by particle breakage. Meanwhile, as shown in Fig. 5, some dusty particles could also be found, suggesting that the surface attrition of particles is also popular under the effects of high compressive force during the survival period of transient and intermittent mechanical jamming.

IV. SIMULATION RESULTS

A. Mechanical jamming

The images of the spread layer of angular particles after spreading are shown in Fig. 6(a), where the particles are colored based on the particle size, i.e., the length of the side of cubes in this work. It could be observed that a number of empty patches are formed within the spread layer. The shape of empty patches is irregular, and their size varies significantly along the spreading direction, which is due to the transient and non-periodically intermittent feature of the mechanical jamming. With the increase in the gap size, both the total area of the empty patches and the maximum size of individual empty patches decrease, which is intuitively expected. It should be noted that even at the gap size of $3.16D$, empty patches also exist, which is much different to the spreading of the particles with almost spherical shape and ignorable rolling friction ($\mu_r = 0.01$) as simulated in Nan *et al.*,¹³ in which there are almost no empty patches when the gap size is larger than $2.11D$. For example, even at the gap size of $2.63D$ ($\delta = 500\,\mu\text{m}$), the empty patches in this work could be as large as $1.76 \times 1.80\,\text{mm}^2$. It suggests that angular particles are easy to get jammed at the bottleneck region, and they are difficult to spread onto the base. Therefore, the critical gap size for the particle flow without any jamming events increases when angular particles are involved. These kinds of large empty patches in Fig. 6(a) are mainly due to the local halting of particle flow caused by mechanical jamming, and their blocky styles are consistent with the ones observed in the experiment in Fig. 4. Correspondingly,

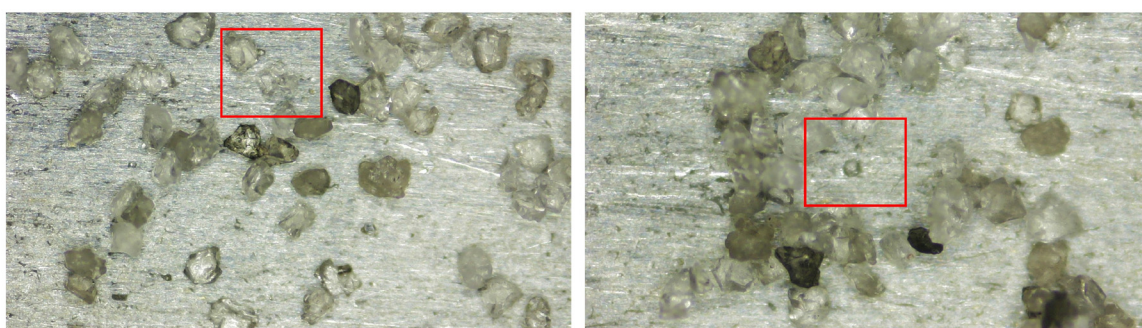


FIG. 5. Breakage of sand particles due to transient and intermittent jamming as observed in the experiment.

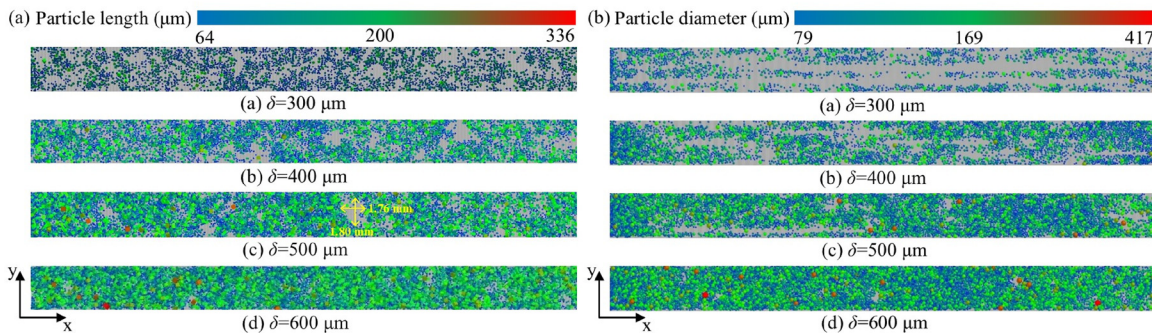


FIG. 6. Snapshots of the deposited particle layer at different gap sizes: (a) an angular particle; (b) a spherical particle, where particles are colored based on the particle size.

compared to small particles, large particles are more difficult to be spread onto the base due to jamming, although their sizes are all smaller than the gap size. For example, at the gap size of 400 μm , the maximum particle size is only $l_p = 255 \mu\text{m}$ with a volume-equivalent diameter of $d_v = 316 \mu\text{m}$. With the increase in gap size, more and more large particles could be spread onto the base.

Compared to angular particles, the spherical particles tend to form elongated empty patches, as shown in Fig. 6(b). This is attributed to their round shape, but with a large rolling friction. Under the effect of a large rolling friction coefficient, the jammed particles could survive for a long time without rolling away from the bottleneck along the spreading direction. However, due to their round shape, the jammed particles tend to slide alone on the base without dragging their neighbors. On the contrary, for angular particles, strong interlocking could be formed between the jammed particles and their neighbors; thus, jammed particles could drag their neighbors to move together with the blade. Meanwhile, due to the counter-dragging effects from their neighbors, the jammed angular particles are usually easily released from the bottleneck region under the stagnation effect of the base, prohibiting the formation of elongated empty patches. Therefore, angular particles tend to block the bottleneck region with a wide space in y direction but survive for a small time, resulting in the formation of blocky-styled empty patches, i.e., the size in both the direction of the width and length is comparable, as shown in Figs. 4 and 6(a), while the spherical particles with large rolling friction resistance tend to block the bottleneck region with a small space in y direction but survive for a long time, resulting in the formation of elongated empty patches, as shown in Figs. 3 and 6(b).

Figure 7 shows the total area percentage of empty patches for angular and spherical particles, which is calculated through the analysis of the images of the spread layer in Fig. 6. To address the sensitivity of the jamming behavior of angular particles and spherical particles to the surface roughness of the base, the cases using a smooth base (i.e., the base is represented by an ideally flat plate) are also included. With the increase in gap size, fewer empty patches are found within the spread layer, which agrees well with the snapshots of the spread layer in Fig. 6. For example, for angular particles, as the gap size increases from $1.58D$ to $3.16D$, the area percentage of empty patches on the rough base decreases from about 58% to 20%. This is also the situation of spherical particles. However, the spreading of spherical particles is more sensitive to the roughness of the base than that of angular particles. For example, at the gap sizes of $1.58D$ and $2.11D$, there are

almost no spherical particles spread onto the smooth base, for which the particle flow is in a full-slip-styled jamming pattern. This is contrary to that of angular particles, for which the interlocking between particles could prevent the jammed particles from slipping on the smooth base to some extent. Therefore, although a large rolling friction coefficient is used for the spherical particles to obtain the same macroscopic flowability as the angular particles, the jamming behavior could be much different, as the jamming structure reported in this work is in the scale of a single particle, which is different from the permanent jamming of the whole particulate system as found in the hopper flow. For both spherical and angular particles, the difference between the rough base and smooth base is reduced as the gap size is increased.

In addition to the empty patches, the difference in the jamming behavior between the angular and spherical particles could be further illustrated by the force chain and the arch structure during the survival time of the jamming event, as shown in Fig. 8. For a clear illustration, only the jammed particles are shown while other particles are hidden. For spherical particles, as shown in Figs. 8(a)–8(c), the jamming structure typically consists of two particles squeezed together and jammed between the blade tip and the base. In contrast, as shown

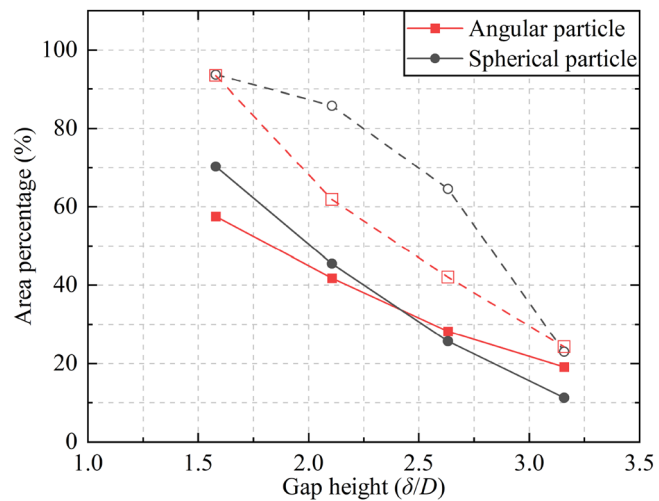


FIG. 7. Total area percentages of empty patches on the rough base (solid symbols) or smooth base (open symbols) for angular particles and spherical particles.

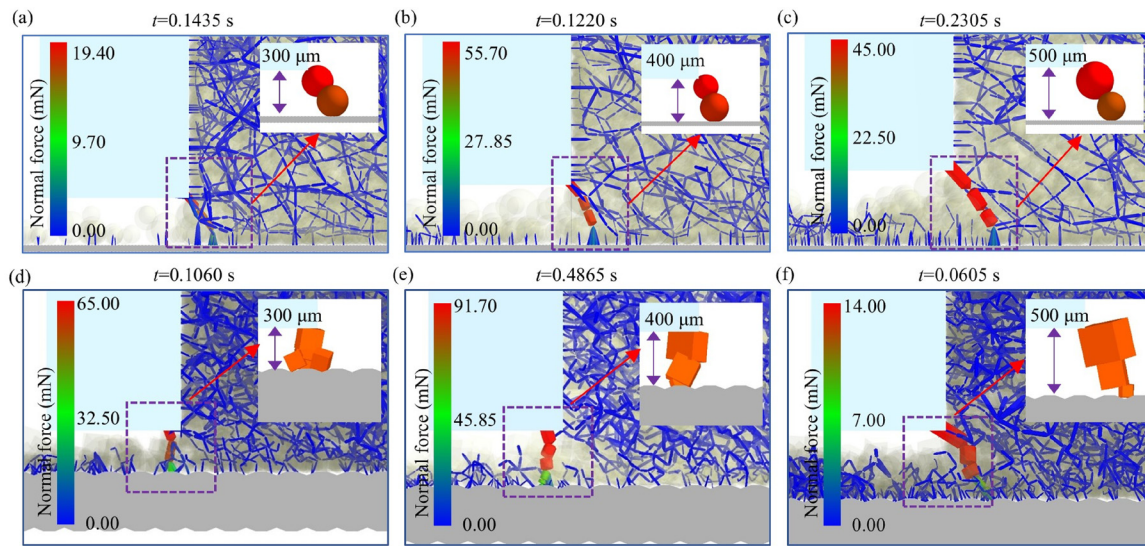


FIG. 8. Snapshots of the force chain and jammed particles for spherical particles (a)–(c) and angular particles (d)–(f) at different gap size: $\delta = 300 \mu\text{m}$ for (a) and (d); $\delta = 400 \mu\text{m}$ for (b) and (e); $\delta = 500 \mu\text{m}$ for (c) and (f).

in Figs. 8(d)–8(f), the jamming structures for angular particles are more diverse due to their geometric shapes, for which the jammed particle could well interlock with the blade and base. These jammed angular particles could be located within the gap between the blade and the base, while underneath the blade, and they can also be squeezed between the blade tip and base when the angular particles try to enter the gap. Figure 8 also shows that the jamming structure usually consists of a few particles instead of a single large particle entirely blocking the bottleneck. Compared to spherical particles, more angular particles are involved and tend to pack together in the jamming structure, which agrees well with the discussions above. For example, as shown in Fig. 8(f), the cubes are jammed like stacking three blocks together and then inserting them into the gap.

B. Shear band

To investigate the local rheological behavior of particles in the shearing region of the blade, a box region in front of the blade is focused, as shown in Fig. 9. It has a length of 1.2 mm in the spreading direction (x direction), a height of 2 mm in the vertical direction (z direction), and the same width (i.e., 3 mm) as the blade in the y direction. The left boundary of the box region is aligned with the front face of the blade, allowing for a focused analysis of the so-called “near-wall bottleneck zone,” where particles are subjected to strong confinement and interfacial interaction with the blade. The box region is divided into several sub-bins along the vertical direction (z direction), and each bin overlaps with its neighboring bins by 50% in the vertical direction (z direction) to enhance statistical smoothness.

Figure 10 shows the distribution of the x component (i.e., spreading direction) of particle velocity along the vertical direction, in which the size of each bin is 0.2 mm in the vertical direction. The particle velocity u_x of each bin is averaged for all particles and then averaged for time. It is normalized by the blade speed U . For both angular and spherical particles, the profile of u_x along the vertical direction has a

similar pattern as reported by Nan and Ghadiri,²⁴ in which the particles with almost spherical shape and ignorable rolling friction ($\mu_r = 0.01$) were used. For example, both findings show that the particle velocity u_x/U increases with the bin center position Z and finally reaches a plateau. Therefore, the particle velocity only shows significant variation at a low vertical position relative to the blade. With the increase in the gap size, the profiles move to the right, and the velocity of particles closest to the base decreases significantly. For all cases in this work, the shear band of particle flow near the base is not fully developed. Even for spherical particles, the particle velocity u_x/U is larger than 0.1 at the $\delta/D = 3.16$, which is much larger than the values (i.e., almost zero) reported for the particles with almost spherical shape

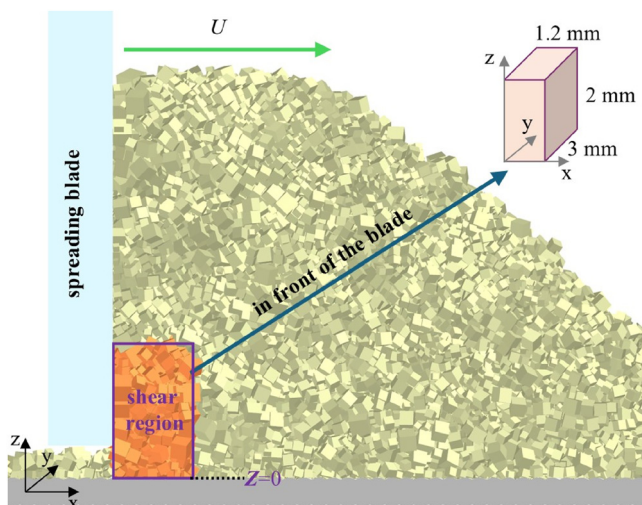


FIG. 9. Illustration of the shear region in front of the moving blade.

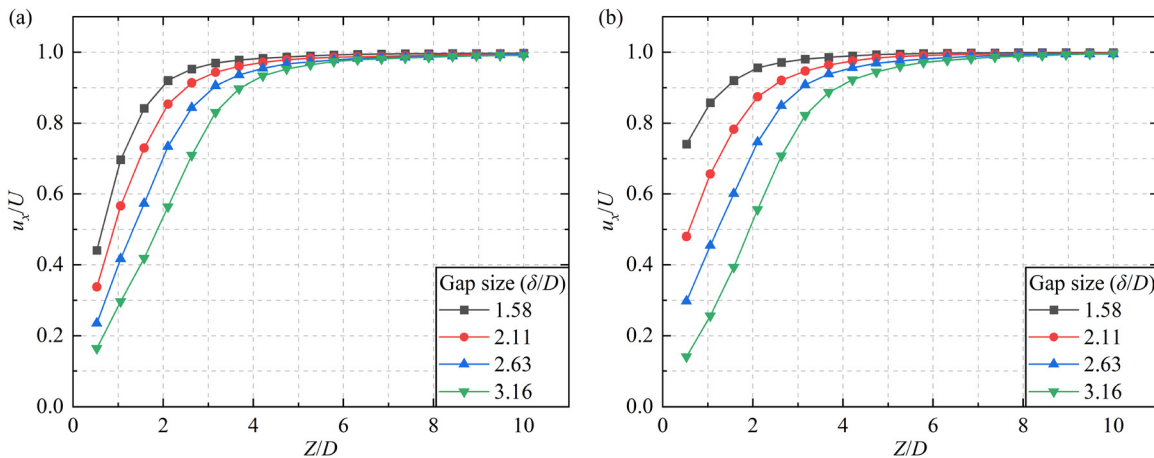


FIG. 10. Distribution of the x component of particle velocity along the vertical direction for (a) an angular particle and (b) a spherical particle.

and ignorable rolling friction ($\mu_r = 0.01$) at a similar gap size in Nan and Ghadiri.²⁴ It suggests that the large rolling friction of particles or the angular geometrical shape of particles promotes a large resistance to the full development of the shear band of particle flow.

Compared to spherical particles, the angular particles exhibit different rheological behavior. Although the angular particles may exhibit a larger interlocking between particles, it seems that they are less dragged by the blade (i.e., less ability to follow up the motion of the blade), while they are more affected by the base. For example, as the gap size δ/D increases from 1.58 to 3.16, the particle velocity at the first bin decreases from 0.74 to 0.14 for spherical particles, while it decreases from 0.44 to 0.16 for angular particles. This is mainly due to the fact that for the angular particles used in this work, i.e., cubes, the blade shearing action does not exert well onto the angular particles close to the base. It could be inferred from the particle stresses described in Sec. IV C, in which the angular particles close to the base bear much less normal and shear stress than spherical particles. Therefore, a lesser blade dragging effect is experienced by the angular particles. These results also demonstrate that the shear band of granular spreading flow mainly exists at the bottleneck region.

Following the same method used in Nan and Ghadiri,²⁴ the velocity profile could be well fitted by the Gauss error function, given as

$$\frac{u_x}{U} = 0.5 \left[1 + \operatorname{erf} \left(\frac{Z - Z_c}{Z_w} \right) \right], \quad (5)$$

$$\operatorname{erf}(x) = \frac{2}{\sqrt{\pi}} \int_0^x e^{-t^2} dt, \quad (6)$$

where $(Z - Z_c)/Z_w$ is the rescaling of the bin center position; Z_c is the center position of the shear band in the vertical direction with respect to the base; Z_w is a linear function of the width of the shear band. When plotting the results of all cases (i.e., a total of eight cases) in this normalized coordinate system, the velocity profiles all collapse onto a universal curve, as shown in Fig. 11. The good agreement between the fitted curve and the simulation results confirms the presence of a well-defined shear zone, further validating the applicability of Gauss error function on the description of the spreading flow of particles. It is

interesting that a similar law of particle velocity could also be found in the split-bottom Couette cell or disk, as reported by Fenistein *et al.*^{28,29} To quantify the fitting accuracy, the average absolute relative error (AARE) is examined for each simulation case, given as

$$\text{AARE} = \frac{1}{N} \sum_{i=1}^N \left| \frac{y_{\text{pre},i} - y_{\text{DEM},i}}{y_{\text{DEM},i}} \right| \times 100\%, \quad (7)$$

where $y_{\text{pre},i}$ and $y_{\text{DEM},i}$ are the values at the i th bin as obtained from the fitting equation [i.e., Eq. (5)] and DEM simulations, respectively; N is the total number of bins along the vertical direction. The AARE averaged for all simulation cases shown in Fig. 11 is 1.6%, suggesting a good fitting accuracy. Meanwhile, it should be noted that the data points in Fig. 11 are mainly restricted to $u_x/U > 0.1$. This is due to the

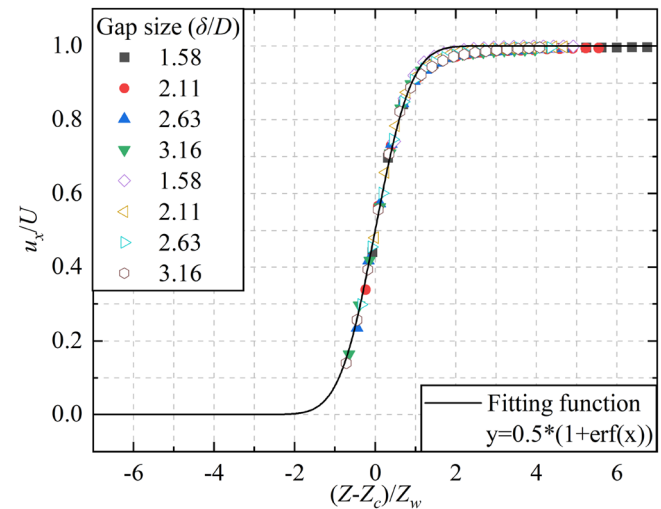


FIG. 11. Universal fitting curve of the distribution of the x component of particle velocity along the vertical direction, in which the solid and open symbols represent the cases using angular and spherical particles, respectively, and the corresponding AARE averaged for all simulation cases is 1.6%.

fact that the shear band reported in this work could not be fully developed, even for the case with a maximum gap size ($\delta/D = 3.16$), resulting in a large velocity of particles in the bin closest to the base, which could be clearly found from Figs. 10 and 11.

The fitting value of the corresponding parameters of the shear band is summarized in Table IV, in which $w = 2.5Z_w$ is used, considering the characteristics of the Gauss error function. The center position of the shear band is more sensitive to the gap size than the particle shape. With the increase in gap size, the center position of the shear band moves to higher vertical positions, which agrees well with the results shown in Fig. 10. For all cases in this work, the center position of the shear band fluctuates around half of the gap size. Correspondingly, for spherical particles, the width of the shear band fluctuates with the increase in gap size, and it is around 5D. However, for angular particles, the width of the shear band increases with the increase in the gap size, indicating that the shear region is much restricted by the stationary base when the gap size is small. The corresponding AARE for each simulation case is also included in Table IV, which has a maximum value of 2.3% and a minimum value of 0.6%, demonstrating that the velocity distribution of particles in the shear band of the granular spreading system could be well described by the Gauss error function [i.e., Eqs. (5) and (6)].

Figure 12 shows the distribution of the vertical component of particle velocity (u_z) along the vertical direction, which is normalized by the characteristic gravity-induced speed ($gD)^{0.5}$. This normalization reflects the balance between gravity and inertial forces in the vertical motion. In almost all cases, at the vertical positions close to the base, the particles show a negative velocity, indicating that the particles are flowing down due to the stagnation effects of the base and the particle weight, and its absolute value increases until reaching a maximum value. At the vertical positions much higher than the base, the velocity would increase from negative to positive as the height of the bins increases, and finally it reaches a plateau, indicating that the particles are pushed upward. The upward motion of the particles (i.e., positive velocity) is mainly due to the pushing effects of the convection flow of the particles within the heap as reported in previous work.¹⁷ Therefore, there exists a separation point in the bottleneck region in terms of particle vertical velocity, as shown in the sub-schematics in Fig. 12(a). For the angular particles, the separation point, i.e., the intersections between the dotted line ($u_z = 0$) and the curves, is below the blade tip in the cases of small gap size, and it moves to a higher position than the blade tip in the cases of large gap size. However, for the spherical particles, the separation point is above the gap size in all cases, for which the underlying mechanism is not clear, and it needs further research in the future.

TABLE IV. Parameters of the shear band of the spreading flow of the angular particle and the spherical particle.

Gap size (δ/D)	Angular particle			Spherical particle		
	Z_c/D	w/D	AARE	Z_c/D	w/D	AARE
1.58	0.62	3.48	1.4%	-0.49	5.33	0.6%
2.11	0.92	4.10	2.0%	0.53	5.05	1.3%
2.63	1.36	4.63	2.3%	1.22	5.05	1.5%
3.16	1.86	5.13	1.9%	1.94	4.93	2.2%

C. Particle stress

For an individual particle in the shear region, its contact stress tensor is given as

$$\sigma_{ij} = \frac{\sum f_{ij} \otimes r_{ij}}{V_p}, \quad (8)$$

where V_p is the volume of an individual particle; f_{ij} is the contact force for each contact point exerted on the particle and r_{ij} is the corresponding branch vector between the mass center of the particle and the contact point. From the full contact stress tensor, the major (σ_1), intermediate (σ_2), and minor (σ_3) principal stresses could be obtained. The normal stress σ and the shear stress τ of an individual particle are then given as

$$\sigma = \frac{\sigma_1 + \sigma_2 + \sigma_3}{3}, \quad (9)$$

$$\tau = \frac{\sqrt{(\sigma_1 - \sigma_2)^2 + (\sigma_1 - \sigma_3)^2 + (\sigma_2 - \sigma_3)^2}}{\sqrt{6}}. \quad (10)$$

To illustrate the distribution of the stresses along the vertical direction, the shear region shown in Fig. 9 is divided into several bins, for which each bin has a size of $2D$ in the vertical direction. For angular particles, as shown in Figs. 13(a) and 13(c), with the increase in the vertical position, the normal stress almost fluctuates around the value which is larger than the hydrostatic pressure. Here, the hydrostatic pressure is calculated by dividing the total particle weight by the area of the heap interacting with the base, i.e., $10 \times 3 \text{ mm}^2$ used in this work, in which 10 mm is a roughly averaged value estimated from the snapshot of the heap during the spreading process. Of course, there is a slight increase for the bins close to the base, but it is almost ignorable. Compared to the angular particles, the stresses of spherical particles show a distinct distribution along the vertical direction, as shown in Figs. 13(b) and 13(d). Apart from the cases with the gap size of $\delta/D = 3.16$, for the bins close to the base, especially for $Z/D < 3.16$, both the normal and shear stresses are much larger than those of angular particles. For example, at the gap size of $\delta/D = 2.11$, the shear stress is 0.42 kPa for spherical particles, while it is 0.26 kPa for angular particles. Meanwhile, with the increase in the vertical position, the stresses of spherical particles show a sharp decrease. Of course, for the region away from the base, i.e., $Z/D > 4.21$, the stresses of spherical particles also fluctuate around a plateau, and the difference of the stresses between the spherical and angular particles is significantly weakened. This indicates that the most critical difference in stress response caused by particle geometric shapes is limited to the near-wall bottleneck region.

To further characterize the local rheological behavior of particle flow in the bottleneck region, the bulk friction coefficient μ_b and the inertial number I are examined, given as

$$I = \dot{\gamma} D \sqrt{\rho_p / \sigma}, \quad (11)$$

$$\mu_b = \frac{\tau}{\sigma}, \quad (12)$$

where $\dot{\gamma}$ is the shear strain rate, and it could be simplified as

$$\dot{\gamma} = \frac{\Delta u_x}{\Delta z}, \quad (13)$$

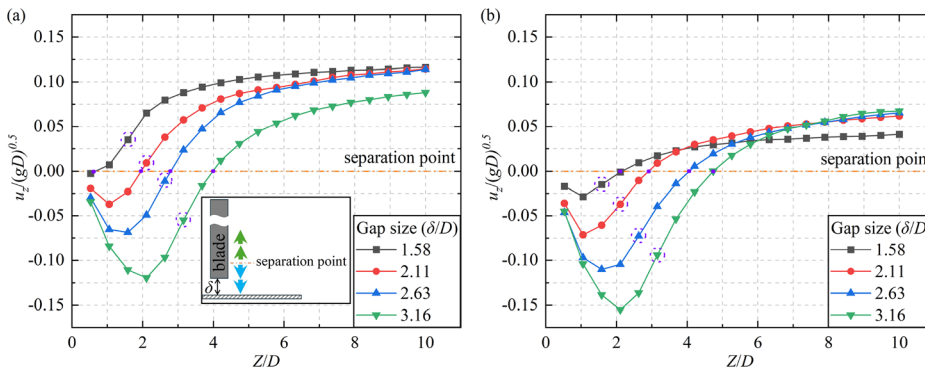


FIG. 12. Distribution of the vertical particle velocity u_z along the vertical direction for (a) an angular particle and (b) a spherical particle, in which the phenomenon of velocity separation exists.

where Δu_x is the velocity difference between two adjacent bins; $\Delta z = D$ is the distance of the centers between two adjacent bins. The variation of the bulk friction coefficient with the inertial number is shown in Fig. 14, in which a logarithmic scale is used for the horizontal axis to better reveal the trends over a broad range of inertial numbers. Here, each data point refers to a value calculated for an individual bin at the specified gap size. It could be found that for both angular and spherical particles, the bulk friction coefficient increases with the inertial number. This is intuitively expected, and it is consistent with the local rheology theory of granular flow.^{30–32} Of course, for spherical particles, a large scattering of the data points is found, which may be due to their spherical shape, but with a large rolling friction, and the underlying mechanism needs further work in the future. It should be noted that the bulk friction coefficient reported in this work is larger than 1.0,

much larger than the ones reported in traditional granular flow systems.^{33,34} Therefore, the large bulk friction coefficient could be deemed as the nature of the granular flow in the spreading system, which is mainly due to the combined effects of the blade shearing and bottleneck effect. Following the law of local rheology used in Nan *et al.*,³⁵ the variation of the bulk friction coefficient could be fitted using the following equation:

$$\mu_b = \mu_s + aI^n, \quad (14)$$

where μ_s is the bulk friction coefficient in the quasi-static regime; a and n are the fitting parameters of the power-law. The fitted values of these parameters are summarized in Table V. It could be found that for both spherical and angular particles used in this work, μ_s and a are almost similar, which maybe due to their similar flowability, i.e.,

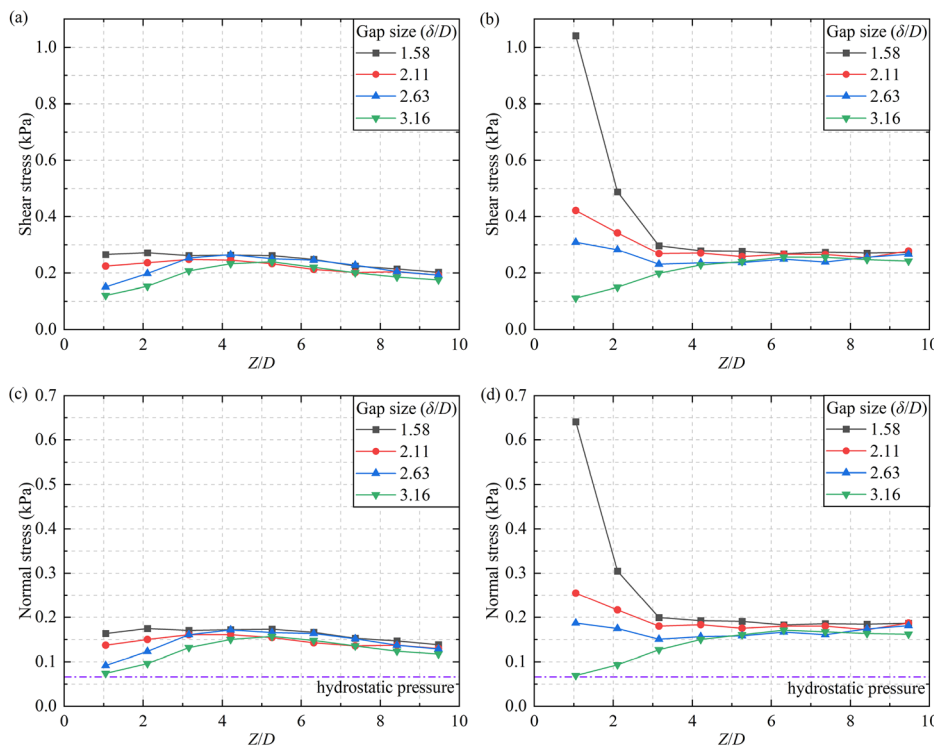


FIG. 13. Distribution of the averaged particle stress in the bottleneck region along the vertical direction: (a) an angular particle, shear stress; (b) a spherical particle, shear stress; (c) an angular particle, normal stress; and (d) a spherical particle, normal stress.

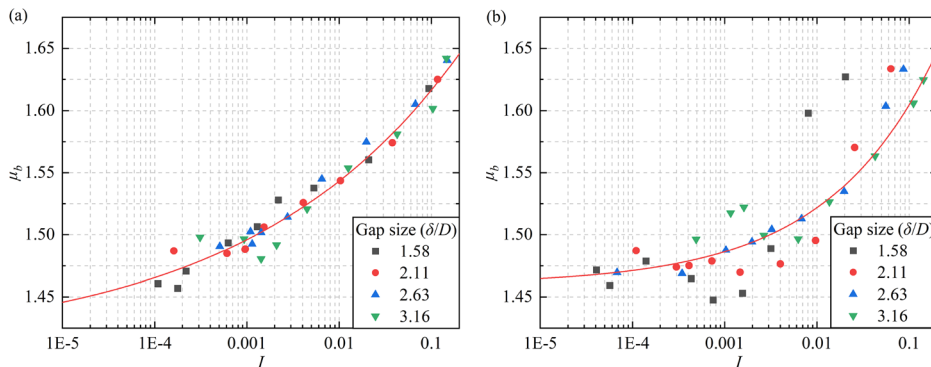


FIG. 14. Variation of the bulk friction coefficient with the inertial number for (a) an angular particle and (b) a spherical particle.

similar repose angle of the particle heap as a large rolling friction coefficient is used for the spherical particles in this work. The exponent index n of the spherical particles is much larger than that of angular particles. For example, the value of n is 0.368 for spherical particles, while it is 0.167 for angular particles, indicating that the spherical particles could respond more sensitively to the variation of the inertial number. Meanwhile, the value of n less than 1.0 is mainly due to the combined effects of the blade shearing and bottleneck effect in this confined granular spreading system. Following the same method as given in Eq. (7), the AARE of the fitting equation using Eq. (14) is examined and included in Table V, which has a maximum value of 1.2%.

In addition to the bulk friction coefficient, the variation of the solid fraction ϕ with the inertial number I is also analyzed, as shown in Fig. 15. It could be observed that the solid fraction decreases monotonically with increasing inertial number for both angular and spherical particles, which is consistent with the well-established dilatancy

behavior of dense granular flows. Following the empirical model proposed by da Cruz *et al.*,³⁶ the solid fraction could be related to the inertial number, given as

$$\phi = \phi_0 - bI^m, \quad (15)$$

where ϕ_0 denotes the asymptotic packing fraction at vanishing shear rate; b and m are the fitting parameters of the power-law. The fitted values of these parameters are summarized in Table VI. Compared to angular particles, the value of b is similar, while the exponent m is larger for spherical particles, suggesting that the solid fraction of spherical particles is more sensitive to the variation of the inertial number. This may be related to the lack of geometric constraints and the enhanced rearrangement capability of spherical particles under increasing shear rate, leading to a stronger dilatancy response. Overall, the fitted model captures the observed trends with reasonable accuracy, as indicated by the AARE, which has a value of 1.6% for angular particles and 1.4% for spherical particles, respectively.

TABLE V. Fitting parameters of the rheological model of the angular particle and the spherical particle.

Particle shape	μ_s	a	n	AARE
Angular particle	1.387	0.343	0.167	0.5%
Spherical particle	1.459	0.339	0.368	1.2%

TABLE VI. Fitting parameters of the solid fraction in the shear band of the angular particle and the spherical particle.

Particle shape	ϕ_0	b	m	AARE
Angular particle	0.607	0.410	0.352	1.6%
Spherical particle	0.574	0.426	0.485	1.4%

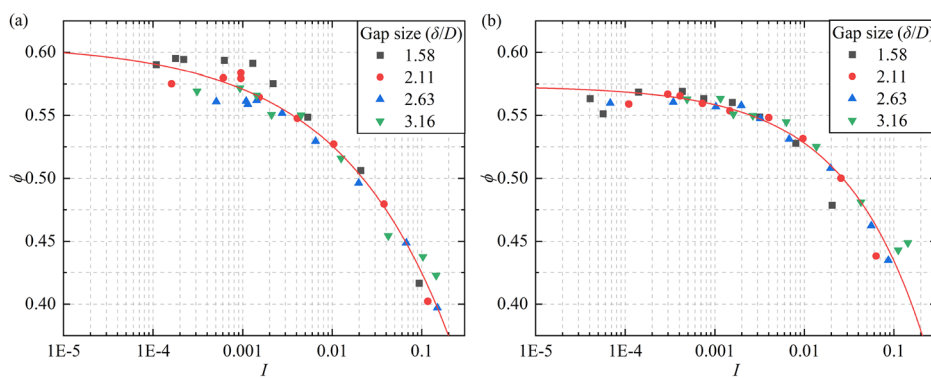


FIG. 15. Variation of the solid fraction coefficient with the inertial number for (a) an angular particle and (b) a spherical particle.

V. CONCLUSIONS

The jamming and rheological behavior of angular particles is explored through experiments and simulation using the Discrete Element Method. The effects of particle shape on particle jamming are analyzed through the empty patches and force chain, followed by the analysis of their sensitivity to the roughness of the base. The rheological behavior of particle flow in the bottleneck region is explored through the velocity profiles and particle stresses, which are followed by the development of their mathematical models. The main results from the present study are summarized as follows:

- (1) Depending on particle shape, different styles of jamming-induced empty patches could be formed. The spread layer has a large tendency to form empty patches with a blocky shape for angular particles, while the elongated shape of empty patches is more prone to spherical particles. The critical gap size for the particle flow without any jamming events increases when angular particles are involved.
- (2) High localized stress formed during the survival period of jamming could even induce the breakage of particles, which is prone for the angular particle in brittle material. Surface attrition of particles is also popular when jamming occurs.
- (3) The interlocking between the particles and the blade or base is important for the mechanical jamming reported in this work. Compared to spherical particles, more angular particles are involved and tend to pack together in the jamming structure. The spreading of spherical particles is more sensitive to the roughness of the base than that of angular particles, especially when the gap is narrow.
- (4) The applicability of the Gauss error function, as previously used in the description of particle velocity in a split-bottom Couette cell or disk, is validated for the shear band in the particle spreading flow. The large rolling friction of particles or the angular shape of particles promotes a large resistance to the full development of the shear band of particle flow.
- (5) A separation point exists in the bottleneck region in terms of particle vertical velocity, and its position depends on the gap size or the vertical position of the blade tip. For the angular particles, the separation point is below the blade tip for the cases with small gap sizes, and it moves to a position higher than the blade tip for the cases with large gap sizes.
- (6) The value of the bulk friction coefficient being larger than 1.0 could be deemed as the nature of granular spreading flow, which is mainly due to the combined effects of the blade shearing and bottleneck effect. In the bottleneck region, the normal and shear stresses of spherical particles are much larger than those of angular particles in the regions close to the base, but their difference is significantly reduced in the regions far away from the base.

ACKNOWLEDGMENTS

The corresponding author is grateful to the National Natural Science Foundation of China (Grant No. 51806099), and thankful to Professor Mojtaba Ghadiri, University of Leeds, UK, for his inspiration on this work.

AUTHOR DECLARATIONS

Conflict of Interest

The authors have no conflicts to disclose.

Author Contributions

Ziming He: Conceptualization (equal); Data curation (equal); Validation (equal); Visualization (equal). **Wenguang Nan:** Conceptualization (equal); Data curation (equal); Formal analysis (lead); Investigation (lead); Methodology (lead); Supervision (lead); Validation (equal); Visualization (equal); Writing – original draft (lead); Writing – review & editing (lead). **Rui Ma:** Conceptualization (supporting). **Lanzhou Ge:** Data curation (equal). **Yi He:** Conceptualization (equal).

DATA AVAILABILITY

The data that support the findings of this study are available from the corresponding author upon reasonable request.

REFERENCES

- ¹S. Luding, "So much for the jamming point," *Nat. Phys.* **12**, 531–532 (2016).
- ²I. Zuriguel, D. R. Parisi, R. C. Hidalgo, C. Lozano, A. Janda, P. A. Gago, J. P. Peralta, L. M. Ferrer, L. A. Pugnaloni, E. Clement, D. Maza, I. Pagonabarraga, and A. Garcimartin, "Clogging transition of many-particle systems flowing through bottlenecks," *Sci. Rep.* **4**, 7324 (2014).
- ³K. To, P.-Y. Lai, and H. K. Pak, "Jamming of granular flow in a two-dimensional hopper," *Phys. Rev. Lett.* **86**, 71–74 (2001).
- ⁴P. P. Behringer, "Jamming in granular materials," *C. R. Phys.* **16**, 10–25 (2015).
- ⁵S. Mondal and M. M. Sharma, "Role of flying buttresses in the jamming of granular matter through multiple rectangular outlets," *Granular Matter* **16**, 125–132 (2014).
- ⁶C. Mankoc, A. Garcimartin, I. Zuriguel, D. Maza, and L. A. Pugnaloni, "Role of vibrations in the jamming and unjamming of grains discharging from a silo," *Phys. Rev. E* **80**, 011309 (2009).
- ⁷M. A. Aguirre, J. G. Grande, A. Calvo, L. A. Pugnaloni, and J. C. Géminard, "Pressure independence of granular flow through an aperture," *Phys. Rev. Lett.* **104**, 238002 (2010).
- ⁸B. De-Song, Z. Xun-Sheng, X. Guang-Lei, P. Zheng-Quan, T. Xiao-Wei, and L. Kun-Quan, "Critical phenomenon of granular flow on a conveyor belt," *Phys. Rev. E* **67**, 062301 (2003).
- ⁹A. Guariguata, M. A. Pascall, M. W. Gilmer, A. K. Sum, E. D. Sloan, C. A. Koh, and D. T. Wu, "Jamming of particles in a two-dimensional fluid-driven flow," *Phys. Rev. E* **86**, 061311 (2012).
- ¹⁰R. P. Behringer and B. Chakraborty, "The physics of jamming for granular materials: A review," *Rep. Prog. Phys.* **82**, 012601 (2019).
- ¹¹D. Pan, Y. Wang, H. Yoshino, J. Zhang, and Y. Jin, "A review on shear jamming," *Phys. Rep.* **1038**, 1–18 (2023).
- ¹²S. Zinatloo Ajabshir, C. Hare, D. Sofia, D. Barletta, and M. Poletto, "Investigating the effect of temperature on powder spreading behaviour in powder bed fusion additive manufacturing process by discrete element method," *Powder Technol.* **436**, 119468 (2024).
- ¹³W. Nan, M. Pasha, T. Bonakdar, A. Lopez, U. Zafar, S. Nadimi, and M. Ghadiri, "Jamming during particle spreading in additive manufacturing," *Powder Technol.* **338**, 253–262 (2018).
- ¹⁴W. Nan, L. Ge, W. Xuan, and Y. Gu, "Transient jamming of granular flow by blade spreading," *Powder Technol.* **431**, 119057 (2024).
- ¹⁵L. Ge, R. Xu, and W. Nan, "Wear of blade spreader during powder spreading in additive manufacturing," *Tribol. Int.* **188**, 108818 (2023).
- ¹⁶M. Y. Shaheen, A. R. Thornton, S. Luding, and T. Weinhart, "The influence of material and process parameters on powder spreading in additive manufacturing," *Powder Technol.* **383**, 564–583 (2021).

- ¹⁷W. Nan, M. Pasha, and M. Ghadiri, "Numerical simulation of particle flow and segregation during roller spreading process in additive manufacturing," *Powder Technol.* **364**, 811–821 (2020).
- ¹⁸A. Phua, C. Doblin, P. Owen, C. H. J. Davies, and G. W. Delaney, "The effect of recoater geometry and speed on granular convection and size segregation in powder bed fusion," *Powder Technol.* **394**, 632–644 (2021).
- ¹⁹Y. Xu, L. Ge, and W. Nan, "Investigation on the spreading behaviour of sand powder used in binder jet 3D printing," *Granular Matter* **26**, 49 (2024).
- ²⁰J. Schindelin, I. Arganda-Carreras, E. Frise, V. Kaynig, M. Longair, T. Pietzsch, S. Preibisch, C. Rueden, S. Saalfeld, B. Schmid, J.-Y. Tinevez, D. J. White, V. Hartenstein, K. Eliceiri, P. Tomancak, and A. Cardona, "Fiji: An open-source platform for biological-image analysis," *Nat. Methods* **9**, 676–682 (2012).
- ²¹P. A. Cundall and O. D. L. Strack, "A discrete numerical model for granular assemblies," *Geotechnique* **29**, 47–65 (1979).
- ²²C. Thornton, *Granular Dynamics, Contact Mechanics and Particle System Simulations: A DEM Study* (Springer, 2015).
- ²³W. Nan, M. Pasha, U. Zafar, S. Nadimi, W. P. Goh, and M. Ghadiri, "Characterisation of gas-atomised metal powders used in binder jet 3D printing," *Powder Technol.* **436**, 119471 (2024).
- ²⁴W. Nan and M. Ghadiri, "Numerical simulation of powder flow during spreading in additive manufacturing," *Powder Technol.* **342**, 801–807 (2019).
- ²⁵B. Nassauer and M. Kuna, "Contact forces of polyhedral particles in discrete element method," *Granular Matter* **15**, 349–355 (2013).
- ²⁶J. Ai, J.-F. Chen, J. M. Rotter, and J. Y. Ooi, "Assessment of rolling resistance models in discrete element simulations," *Powder Technol.* **206**, 269–282 (2011).
- ²⁷W. Xuan and W. Nan, "Analysis on the mechanical jamming of particle flow using impeller-based rheometer," *Powder Technol.* **444**, 120003 (2024).
- ²⁸D. Fenistein and M. van Hecke, "Wide shear zones in granular bulk flow," *Nature* **425**, 256–256 (2003).
- ²⁹D. Fenistein, J. W. van de Meent, and M. van Hecke, "Universal and wide shear zones in granular bulk flow," *Phys. Rev. Lett.* **92**, 094301 (2004).
- ³⁰G. Koval, J. N. Roux, A. Corfdir, and F. Chevoir, "Annular shear of cohesionless granular materials: From the inertial to quasistatic regime," *Phys. Rev. E* **79**, 021306 (2009).
- ³¹J. Hao and Y. Guo, "Rheology of sheared polyhedral granular materials in inclined flows," *Phys. Fluids* **35**, 103310 (2023).
- ³²W. J. Han, H. Zhao, and D. M. Wang, "Particle fluctuations and their effects on the rheological behavior of sheared granular flows," *Phys. Fluids* **35**, 063304 (2023).
- ³³P. Jop, Y. Forterre, and O. Pouliquen, "A constitutive law for dense granular flows," *Nature* **441**, 727–730 (2006).
- ³⁴G. D. R. MiDi, "On dense granular flows," *Eur. Phys. J. E* **14**, 341–365 (2004).
- ³⁵W. Nan, M. Pasha, and M. Ghadiri, "Rheology of a dense granular bed penetrated by a rotating impeller," *Powder Technol.* **386**, 60–69 (2021).
- ³⁶F. da Cruz, S. Emam, M. Prochnow, J. N. Roux, and F. Chevoir, "Rheophysics of dense granular materials: Discrete simulation of plane shear flows," *Phys. Rev. E* **72**, 021309 (2005).